Chapter 25
Multifractal Analysis of Brain Tumor Interface in Glioblastoma

Jacksson Sánchez and Miguel Martín-Landrove

Abstract The dynamics of tumor growth is a very complex process, generally accompanied by numerous chromosomal aberrations that determine its genetic and dynamical heterogeneity. Consequently, the tumor interface exhibits a non-regular and heterogeneous behavior often described by a single fractal dimension. A more suitable approach is to consider the tumor interface as a multifractal object that can be described by a set of generalized fractal dimensions. In the present work, detrended fluctuation and multifractal analysis are used to characterize the complexity of glioblastoma.

Keywords Multifractal · Glioblastoma · Fractal dynamics · Complexity

25.1 Introduction

Multifractal and detrended fluctuation analysis has been used for the evaluation of the texture in medical image analysis [1–3]. In particular, it has been used for brain tumor classification and grading [4–7], brain tumor segmentation through the characterization of image texture [8–14], and as a radiomic feature [15–20]. Fractal dimension has been used as a prime feature associated with image intensity to detect and classify brain tumors [21, 22], characterize brain tumor microvascularity [23, 24] and in IoT developments [25]. In all of the previously mentioned approaches, the derived fractal quantities give information on the bulk tumor growth dynamics and heterogeneity. A different approach to studying the

J. Sánchez
Faculty of Science and Technology, Physics Department, Universidad Nacional Pedro Henríquez Ureña, Santo Domingo, Dominican Republic
e-mail: jsanchez@unphu.edu.do

M. Martín-Landrove (✉)
Centre for Medical Visualization, National Institute for Bioengineering, INABIO, Universidad Central de Venezuela and Centro de Diagnóstico Docente Las Mercedes, Caracas, Venezuela
e-mail: mmartin@cddlasmercedes.com

A. Di Ieva (ed.), *The Fractal Geometry of the Brain*, Advances in Neurobiology 36,
https://doi.org/10.1007/978-3-031-47606-8_25

dynamics of tumor growth comes from the fractal and scaling analysis of the tumor interface as originally proposed by Brú et al. [26–29] *in vitro* and *ex vivo* tumor samples. Application of fractal and scaling analysis to the tumor interface for *in vivo* contrast-enhanced T_1 weighted MRI of brain tumors was first done by Martín-Landrove and Pereira [30]. The analysis was further extended to three-dimensional contrast-enhanced T_1-weighted MRI of brain images [31–33]. In this chapter, a general approach based on multifractal and detrended fluctuations analysis is used to characterize fluctuations of quantities supported on the tumor interface, such as the radius, interface width, and contrast-enhanced image intensity.

25.2 Image Selection and Segmentation

Images for glioblastoma were extracted from collections in The Cancer Imaging Archive [34, 35], the TCGA-GBM collection [36] and from the RSNA-ASNR-MICCAI Brain Tumor Segmentation (BraTS) Challenge 2021 [37–39], which includes a classification according to O(6)-methylguanine-DNA methyltransferase (MGMT) promoter methylation [40, 41]. Among these collections, T_1-weighted images, either contrast-enhanced or not, were selected and further reviewed. Tumor lesions selected for image processing were identified as such and separated from anatomical structures.

Images were segmented according to a dynamical quantum clustering algorithm [42, 43] applied to medical image data [44–46].

25.3 Multifractal Analysis

To determine the multifractal scaling exponents for the one-dimensional ordered series extracted from the tumor interface, as seen in Fig. 25.1, a general procedure of fluctuation analysis is used [47, 48]. In the following, the method is derived for the ordered series corresponding to the radii of the interface points but it can be

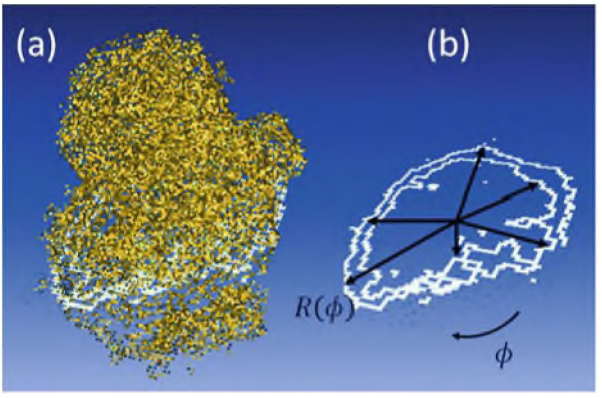

Fig. 25.1 (**a**) Tumor interface point cloud as extracted by the segmentation method previously described; white interface points correspond to a particular slice. (**b**) Construction of the ordered series from points extracted from the tumor interface, in this case, the radius $R(\phi)$

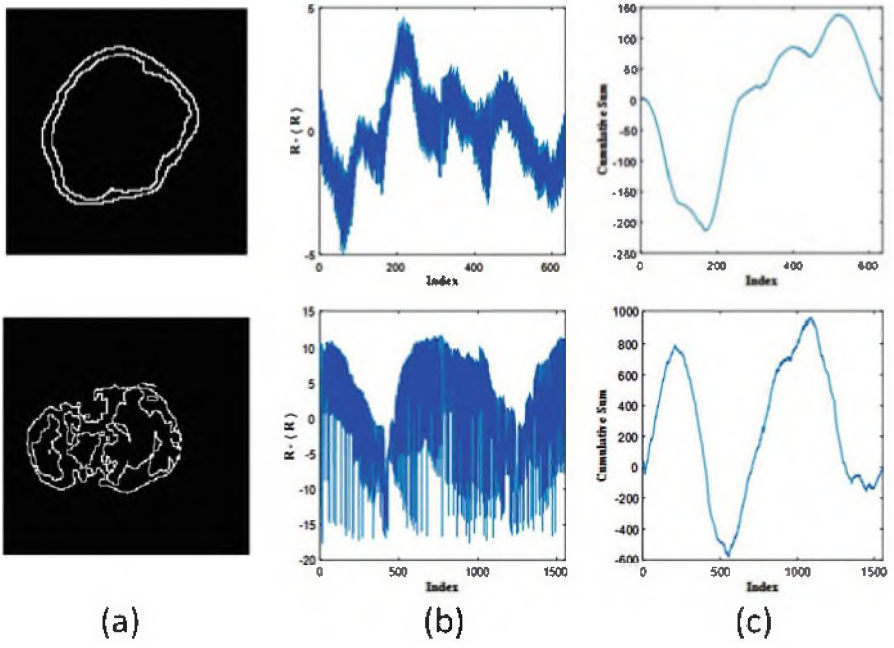

Fig. 25.2 Some examples of extracted ordered series. (**a**) Tumor interface point cloud corresponding to a slice. (**b**) Ordered series of the fluctuations of the radii of the tumor interface and (**c**) the cumulative sum of the ordered series

easily extended to any variable associated with these points such as the average interface width or its contrast-enhanced intensity. First, the profile of the ordered series is determined by a cumulative sum,

$$R(i) \equiv \sum_{k=1}^{i} (r_k - \langle r \rangle) \tag{25.1}$$

where $\langle r \rangle$ represents the mean radius of the tumor interface (see Fig. 25.2). The profile series is then partitioned into $N_s \equiv int(N/s)$ segments of equal length s, the box probability $p_s(v)$, which is the sum of the values r_k within each segment v of size s, is defined as

$$p_s(v) \equiv R(vs) - R((v-1)s) \tag{25.2}$$

The scaling properties and exponents can be obtained through the partition function

$$Z_q(s) \equiv \sum_{v=1}^{N_s} |p_s(v)|^q \tag{25.3}$$

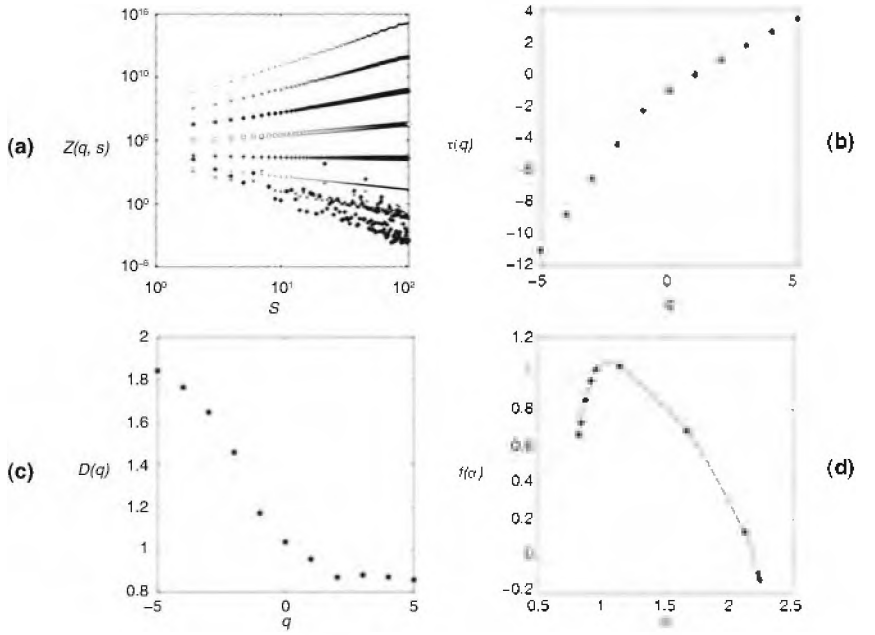

Fig. 25.3 Different steps in multifractal analysis for one-dimensional ordered series extracted from the tumor interface. (**a**) Partition functions $Z_q(s)$. (**b**) Large scale exponents $\tau_1(q)$. (**c**) Generalized fractal dimensions, $D_1(q)$, and (**d**) Singularity spectrum $f_1(\alpha)$

For large values of s, a power law behavior is obtained for $Z_q(s)$ (Fig. 25.3a), allowing for a definition of the scaling exponent $\tau_1(q)$ that characterizes the one-dimensional fluctuations,

$$Z_q(s) \sim s^{\tau_1(q)} \tag{25.4}$$

as seen in Fig. 25.3b.

The generalized fractal dimensions (Fig. 25.3c) are then defined as

$$D_1(q) \equiv \frac{\tau_1(q)}{q-1} \tag{25.5}$$

and the generalized one-dimensional Hurst exponents can be obtained from the relation

$$\tau_1(q) = qh_1(q) - 1 \tag{25.6}$$

A complementary way to characterize the multifractal tumor interface is by determining the singularity spectrum $f_1(\alpha_1)$ (Fig. 25.3d), which is related to $\tau_1(q)$

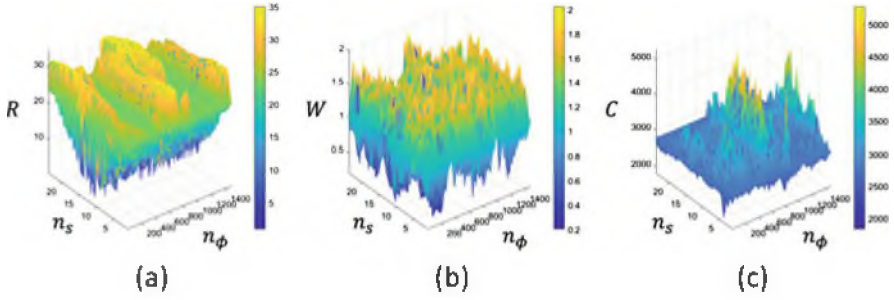

Fig. 25.4 Two-dimensional arrays from the tumor interface. (**a**) Radii extracted from the tumor interface point cloud. (**b**) Fluctuations of the radii for a fixed scale and (**c**) contrast-enhanced image intensity at the tumor interface

by a Legendre transform

$$\alpha_1 = \frac{d\tau_1}{dq},$$
$$f_1(\alpha_1) = q\alpha_1 - \tau_1(q) \tag{25.7}$$

The ordered series that can be extracted from any slice represents a one-dimensional sampling of the tumor interface and as a consequence an incomplete picture of the tumor interface fluctuations. A more general approach is possible if a two-dimensional detrended fluctuation analysis [49] is performed. In this case, the tumor interface is parameterized as a two-dimensional array with elements $r(n_\phi, n_Z)$, the radii of the tumor interface, or any other quantity associated with it, as shown in Fig. 25.4, and is partitioned in two-dimensional segments of size s.

The detrended fluctuation function in each segment is given by

$$F^2(v, w, s) = \frac{1}{s^2} \sum_{i=1}^{s} \sum_{j=1}^{s} \epsilon^2_{v,w}(i, j) \tag{25.8}$$

where $\epsilon_{v,w}(i, j)$ is the difference between the cumulative sum of $r(i, j)$ and its trend over the segment (v, w). The average of the detrended fluctuation over all the segments is

$$F_q(s) = \left\{ \frac{1}{M_s N_s} \sum_{v=1}^{M_s} \sum_{w=1}^{N_s} |F(v, w, s)|^q \right\}^{\frac{1}{q}} \tag{25.9}$$

for $q \neq 0$ and for $q = 0$,

$$F_0(s) = exp\left\{ \frac{1}{M_s N_s} \sum_{v=1}^{M_s} \sum_{w=1}^{N_s} ln[F(v, w, s)] \right\} \tag{25.10}$$

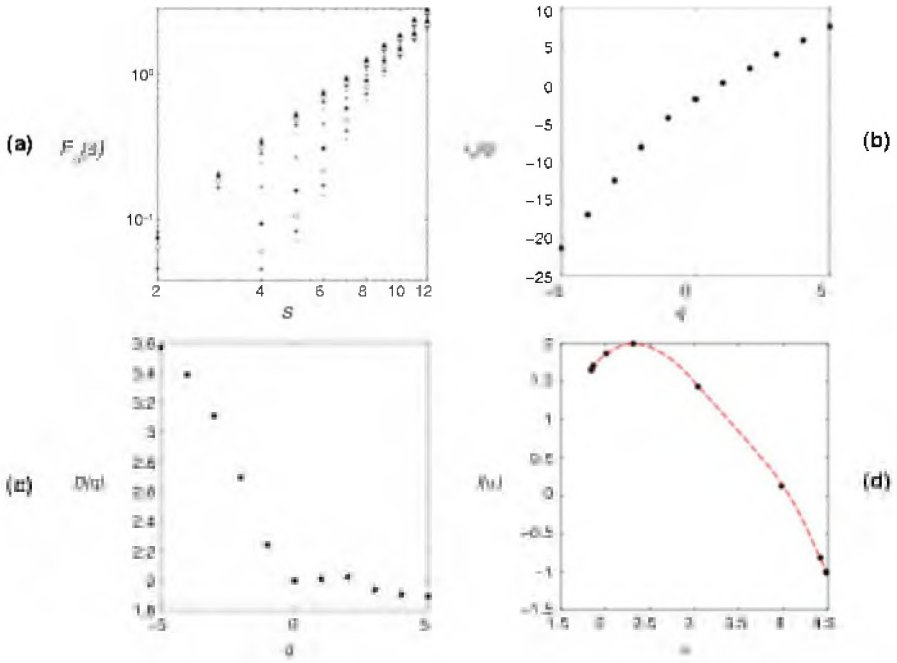

Fig. 25.5 Different steps in detrended fluctuation analysis for two-dimensional arrays extracted from the tumor interface. (**a**) Detrended fluctuation functions $F_q(s)$. (**b**) Large scale exponents $\tau_2(q)$. (**c**) Generalized fractal dimensions. $D_2(q)$, and (**d**) Singularity spectrum $f_2(\alpha)$

For large values of s, F_q behaves as a power law,

$$F_q(s) \sim s^{h_2(q)} \tag{25.11}$$

The multifractal nature of the fluctuation is characterized by the scaling exponents $\tau_2(q)$ and related to the generalized two-dimensional Hurst exponents $h_2(q)$ by

$$\tau_2(q) = qh_2(q) - 2 \tag{25.12}$$

and Eq. 25.5 holds for the generalized fractal dimensions $D_2(q)$. In a similar way, as in Eq. 25.7, the singularity spectrum $f_2(\alpha_2)$ can be determined. The general scheme is presented in Fig. 25.5.

25.4 Results and Discussion

25.4.1 *Multifractal Analysis of One-Dimensional Ordered Series*

The results corresponding to the multifractal analysis of the one-dimensional ordered series are summarized in Table 25.1 showing the average value of the information dimension $D_1(1)$, the correlation dimension $D_1(2)$, and the Hurst exponent, $h_1(2)$.

Also from Table 25.1, the generalized fractal dimension $D_1(0)$, which corresponds to the Euclidean dimension, is very close to 1, as it should be since the ordered series is one-dimensional. Comparison of the values for $D_1(1)$, $D_1(2)$, and $h_1(2)$ among the MGMTp(0) (unmethylated) and MGMTp(1) (methylated) groups yields to the result that both groups are very similar in these quantities, with an increase in favor of the MGMTp(0) group. Also, the Gbm group, which belongs to the TCGA-GBM collection, exhibits results that are very close to the other groups, possibly because this group represents an unknown mixture of unmethylated and methylated MGMT promoters. The general behavior can be seen in Fig. 25.6.

Table 25.1 Generalized fractal dimensions D_q and Hurst exponent, $h_1(2)$ for the one-dimensional ordered series of the radii extracted from the tumor interface

Data set	$D_1(0)$	$D_1(1)$	$D_1(2)$	$h_1(2)$
MGMTp (0)[a]	1.037 ± 0.002	0.90 ± 0.05	0.76 ± 0.11	0.88 ± 0.05
MGMTp (1)[a]	1.036 ± 0.002	0.89 ± 0.06	0.73 ± 0.12	0.86 ± 0.06
Gbm[b]	1.037 ± 0.002	0.88 ± 0.05	0.73 ± 0.10	0.87 ± 0.05

[a] RSNA-ASNR-MICCAI Brain Tumor Segmentation (BraTS) Challenge 2021. (0) Unmethylated MGMT promoter. (1) methylated MGMT promoter

[b] The Cancer Imaging Archive TCGA-GBM collection

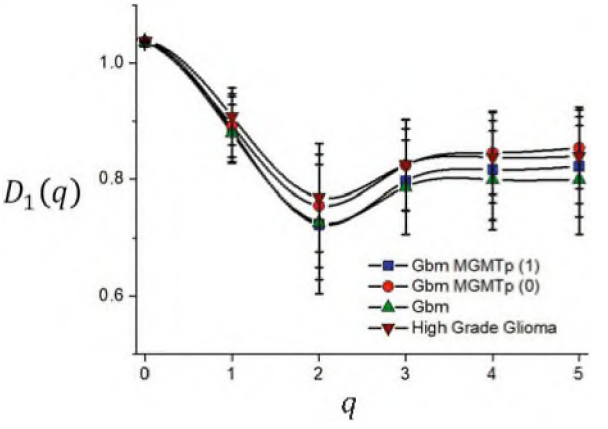

Fig. 25.6 Generalized fractal dimensions $D_1(q)$, associated with one-dimensional ordered series for data sets of glioblastoma and high-grade gliomas

25.4.2 Detrended Fluctuation Analysis of Two-Dimensional Tumor Interface Data

Different data were extracted from the tumor interface: the set of radii of the interface points, R, the set of the interface points fluctuations for a fixed scale, that is, a width evaluated on each interface point, W, and the set of contrast-enhanced image intensities evaluated at each interface point, I. The results for the average value of $D_2(1)$, $D_2(2)$, and $h_2(2)$ are summarized in Table 25.2. Notice in general that all the quantities decrease as the data set is changed from $R \rightarrow W \rightarrow I$ and an increase in favor of the methylated group MGMTp(1) for all the data sets.

The relationship between the generalized fractal dimensions is shown in Fig. 25.7.

25.4.3 Generalized Hurst Exponents and Singularity Spectra

A complementary view of the multifractal nature of the tumor interface can be obtained by the evaluation of the generalized Hurst exponents $h(q)$ and the singularity spectrum $f(\alpha)$. In Tables 25.1 and 25.2, the quantity known as the Hurst exponent, that is, $h(2)$ is evaluated, indicating how correlated the fluctuations in the tumor interface are, but as seen in Fig. 25.8, the dependence on q of the generalized Hurst exponents is more pronounced for $q < 0$ (more sensitive to small fluctuations). This behavior is observed both for the multifractal one-dimensional analysis and for the two-dimensional detrended fluctuation analysis with the possibility to discriminate between the glioblastoma groups.

Table 25.2 Generalized fractal dimensions D_2 and Hurst exponent, $h_2(2)$ for two-dimensional arrays extracted from the tumor interface. R interface radius, W interface width, I contrast image intensity at the interface

Data set	$D_2(1)$	$D_2(2)$	$h_2(2)$
R MGMTp (0)[a]	1.91 ± 0.18	1.82 ± 0.35	1.92 ± 0.17
W MGMTp (0)[a]	1.87 ± 0.21	1.73 ± 0.43	1.87 ± 0.21
I MGMTp (0)[a]	1.84 ± 0.24	1.69 ± 0.48	1.84 ± 0.24
R MGMTp (1)[a]	1.95 ± 0.17	1.90 ± 0.34	1.95 ± 0.17
W MGMTp (1)[a]	1.90 ± 0.17	1.80 ± 0.35	1.90 ± 0.17
I MGMTp (1)[a]	1.88 ± 0.18	1.75 ± 0.36	1.88 ± 0.18
R Gbm[b]	1.93 ± 0.15	1.87 ± 0.30	1.93 ± 0.15
W Gbm[b]	1.88 ± 0.14	1.76 ± 0.28	1.88 ± 0.14
I Gbm[b]	1.86 ± 0.13	1.72 ± 0.26	1.86 ± 0.13

[a] RSNA-ASNR-MICCAI Brain Tumor Segmentation (BraTS) Challenge 2021. (0) Unmethylated MGMT promoter, (1) methylated MGMT promoter

[b] The Cancer Imaging Archive TCGA-GBM collection

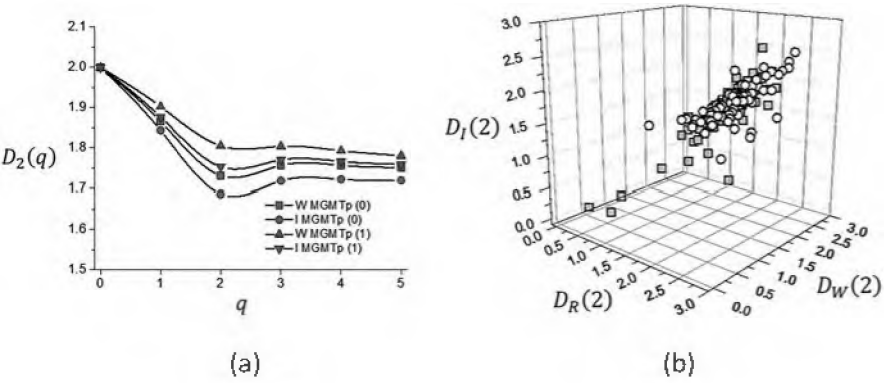

Fig. 25.7 (**a**) Generalized fractal dimensions $D_2(q)$, associated with two-dimensional data arrays extracted from the tumor interface and corresponding to the width of the interface at a certain scale, W, and the contrast-enhanced image intensity, I,; (0) corresponds to unmethylated MGMT promoter and (1) to methylated MGMT promoter. (**b**) Relationship between the correlation dimensions $D_R(2)$, $D_W(2)$ and $D_I(2)$ with MGMTp(0) in square symbols and MGMTp(1) in circles

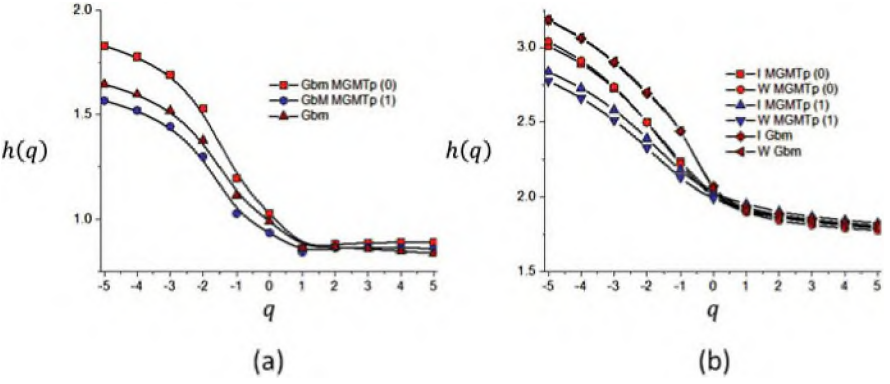

Fig. 25.8 Generalized Hurst exponents, $h(q)$. (**a**) Results obtained by multifractal analysis applied upon one-dimensional ordered series extracted from the tumor interface. (**b**) Results obtained by two-dimensional detrended fluctuation analysis applied upon two-dimensional arrays of interface data; I corresponds to contrast-enhanced image intensity while W is the width of the tumor interface at a fixed scale. (0) corresponds to unmethylated MGMT promoter, (1) to methylated MGMT promoter

Figure 25.9 shows the corresponding singularity spectra obtained by multifractal analysis on one-dimensional ordered series, Fig. 25.9a and two-dimensional detrended fluctuation analysis, Fig. 25.9b.

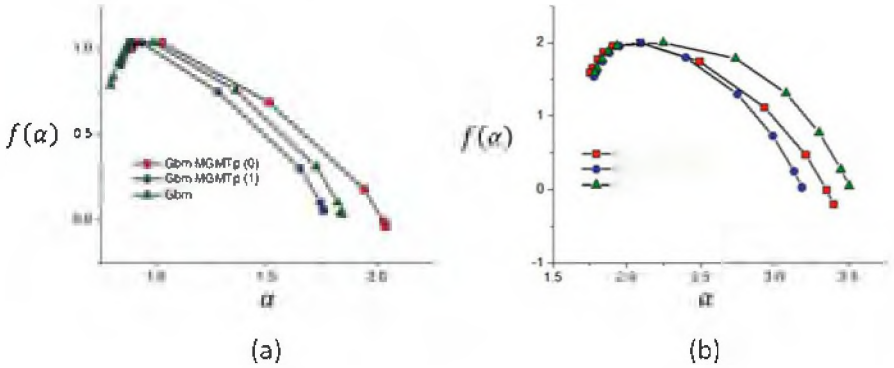

Fig. 25.9 Singularity spectrum $f(\alpha)$. (**a**) Results obtained by multifractal analysis applied upon one-dimensional ordered series of the radii extracted from the tumor interface. (**b**) Results obtained by two-dimensional detrended fluctuation analysis applied upon the two-dimensional array of the radii extracted from the tumor interface. (0) corresponds to unmethylated MGMT promoter, (1) to methylated MGMT promoter

25.5 Conclusions

Multifractal and detrended fluctuation analysis are powerful tools to characterize the heterogeneity and complexity of the tumor interface. The determination of generalized fractal dimensions, generalized Hurst exponents, and related quantities such as singularity spectra besides the commonly used fractal dimension could greatly improve the description of the tumor growth dynamics. From a practical point of view, these quantities add up to the standard set of radiomic features that can be used as discriminators or image biomarkers for tumor detection and classification.

Acknowledgments This research was supported by Universidad Central de Venezuela, INABIO, and Universidad Nacional Pedro Henríquez Ureña. We thank our colleagues from these institutions who provided insight and expertise that greatly assisted the research.

References

1. Lopes R, Dubois P, Bhouri I, Bedoui MH, Maouche S, Betrouni N. Local fractal and multifractal features for volumic texture characterization. Pattern Recognit. 2011;44:1690–7
2. Oudjemia S, Girault J-M, Derguini N, Haddab S. Multifractal analysis: application to medical imaging. In: 2013 8th international workshop on systems, signal processing and their applications (WoSSPA). 2013. p. 244–9
3. Jelinek HF, Milosević NT, Karperien A, Krstonošić B. Box-counting and multifractal analysis in neuronal and glial classification. In: Dumitrache L. (editors) Advances in intelligent control systems and computer science. Advances in intelligent systems and computing, vol 187. Berlin: Springer; 2013. p. 177–89

4. Reza SMS, Mays R, Iftekharuddin KM. Multifractal detrended fluctuation analysis shows promise for brain tumor grading. In: Proceedings of imaging systems and applications 2014. IW4C; 2014
5. Reza SMS, Mays R, Iftekharuddin KM. Multi-fractal detrended texture feature for brain tumor classification. In: Proceedings of the SPIE 9414, medical imaging 2015: computer-aided diagnosis; 2015. p. 941410
6. Reza SMS, Samad MD, Shboul ZA, Jones KA, Iftekharuddin KM. Glioma grading using structural magnetic resonance imaging and molecular data. J Med Imaging. 2019;6:024501
7. Wang J, Shao W, Kim J. Automated classification for brain MRIs based on 2D MF-DFA method. Fractals. 2020;28:2050109
8. Islam A, Reza SMS, Iftekharuddin KM. Multifractal texture estimation for detection and segmentation of brain tumors. IEEE Trans Biomed Eng. 2013;60:3204–3215
9. Reza S, Iftekharuddin KM. Multi-class abnormal brain tissue segmentation using texture features. In: Proceedings NCI MICCAI-BRATS; 2013. p. 38–42
10. Reza S, Iftekharuddin KM. Multi-fractal texture features for brain tumor and edema segmentation. In: Proceedings volume 9035, medical imaging 2014: computer-aided diagnosis; 2014. p. 903503
11. Reza SMS, Islam A, Iftekharuddin KM. Texture estimation for abnormal tissue segmentation in brain MRI. In: Di Ieva A. (editors) The fractal geometry of the brain. Springer series in computational neuroscience; 2016. p. 333–49
12. Lahmiri S. Glioma detection based on multi-fractal features of segmented brain MRI by particle swarm optimization techniques. Biomed Signal Process Control. 2017;31:148–55
13. Islam A, Iftekharuddin KM, Ogg RJ, Laningham FH, Sivakumar B. Multifractal modeling, segmentation, prediction, and statistical validation of posterior fossa tumors. In: Proceedings volume 6915, medical imaging 2008: computer-aided diagnosis; 2008. p. 69153C
14. Khider M, Haddad B. Local multifractal analysis by 2D-WTMM method to detect brain tumor. In: 2013 UKSim 15th international conference on computer modelling and simulation; 2013. p. 461–4
15. Reza SMS, Samad MD, Shboul ZA, Jones KA, Iftekharuddin KM. Glioma grading using structural magnetic resonance imaging and molecular data. J Med Imaging. 2019;6:024501
16. Gilanie1 G, Bajwa UI, Waraich MM, Anwar MW, Ullah H. An automated and risk free WHO grading of glioma from MRI images using CNN. Multimedia tools and applications; 2022. https://doi.org/10.1007/s11042-022-13415-9
17. Farzana W, Shboul ZA, Temtam A, Iftekharuddin KM. Uncertainty estimation in classification of mgnt using radiogenomics for glioblastoma patients. In: K. Drukker, K.M. Iftekharuddin, H. Lu, M.A. Mazurowski, C. Muramatsu, R.K. Samala, editors. Proceedings of SPIE, medical imaging 2022: computer-aided diagnosis 120331E (1–7). Bellingham: Society of Photo-Optical Instrumentation Engineers; 2022
18. Abd-Ellaha MK, Awadb AI, Khalafd AAM, Hamedd HFA. A review on brain tumor diagnosis from MRI images: practical implications, key achievements, and lessons learned. Magn Reson Imaging. 2019;61:300–318
19. Pei L, Bakas S, Vossough A, Reza SMS, Davatzikos C, Iftekharuddin KM. Longitudinal brain tumor segmentation prediction in MRI using feature and label fusion. Biomed Signal Process Control. 2020;55:101648
20. Sadique MS, Temtam A, Lappinen E, Iftekharuddin KM. Radiomic texture feature descriptor to distinguish recurrent brain tumor from radiation necrosis using multimodal MRI. In: Proceedings SPIE 12033, medical imaging 2022: computer-aided diagnosis; 2022. p. 1203321
21. Zook JM, Iftekharuddin KM. Statistical analysis of fractal-based brain tumor detection algorithms. Magn Reson Imaging. 2005;23:671–8
22. Di Ieva A, God S, Grabner G, Grizzi F, Sherif C, Matula C, Tschabitscher M, Trattnig S. Three-dimensional susceptibility-weighted imaging at 7 T using fractal-based quantitative analysis to grade gliomas. Neuroradiology 2013;55:35–40

23. Di Ieva A, Grizzi F, Sherif C, Matula C, Tschabitscher M, Angioarchitectural heterogeneity in human glioblastoma multiforme: a fractal-based histopathological assessment. Microvasc Res 2011;81:222–230
24. Di Ieva A, Bruner E, Widhalm G, Minchev G, Tschabitscher M, Grizzi F. Computer-assisted and fractal-based morphometric assessment of microvascularity in histological specimens of gliomas. Sci Rep 2012;2:429
25. Lenka S, Kumar S, Mishra S, Jena KK. An IoT-cloud based fractal model for brain tumor image analysis. In: Proceedings of the fourth international conference on I-SMAC (IoT in social, mobile, analytics and cloud) (I-SMAC); 2020. p. 1–7
26. Brú A, Pastor JM, Fernaud I, Brú I, Melle S, Berenguer C. Super-rough dynamics on tumor growth. Phys Rev Lett. 1998;81:4008–11
27. Brú A, Albertos S, Subiza JL, López García-Asenjo J, Brú. The universal dynamics of tumor growth. Biophys J. 2003;85:2948–2961
28. Brú A, Casero D, de Franciscis A, Herrero MA. Fractal analysis and tumour growth. Math Comput Modell. 2008;47:546–559
29. Brú. Alós E, Nuño JC, Fernández de Dios M. Scaling in complex systems: a link between the dynamics of networks and growing interfaces. Sci Rep. 2014;4:7550
30. Martín-Landrove M, Pereira D. Fractal properties and critical exponents in tumor. Ciencia. 2008;16:203–7
31. Torres Hoyos F, Martín-Landrove M. 3-D in vivo brain tumor geometry study by scaling analysis. Phys A Stat Mech Its Appl 2012;391:1195–206
32. Martín-Landrove M, Brú A, Rueda-Toicen A, Torres-Hoyos F. Tumor growth in the brain: complexity and fractality. In: Di Ieva A, editors. The fractal geometry of the brain. Springer series in computational neuroscience. New York; Springer; 2016
33. Martín-Landrove M, Torres-Hoyos F, Rueda-Toicen A. Complexity of brain tumors. Phys A: Stat Mech Its Appl 2020;537:122696
34. Chang H, Fontenay GV, Han J, Cong G, Baehner FL, Gray W, Spellman PT, Parvin B. Morphometic analysis of TCGA glioblastoma multiforme. BMC Bioinfor 2011;12:484
35. Clark K, Vendt B, Smith K, Freymann J, Kirby J, Koppel P, Moore S, Phillips S, Maffitt D, Pringle M, Tarbox L, Prior F. The cancer imaging archive (TCIA): maintaining and operating a public information repository. Digit Imaging 2013;26:1045–57
36. Scarpace L, Mikkelsen T, Cha S, Rao S, Tekchandani S, Gutman D, Saltz JH, Erickson BJ, Pedano N, Flanders AE, Barnholtz-Sloan J, Ostrom Q, Barboriak D, Pierce LJ. Radiology data from the cancer genome atlas glioblastoma multiforme [TCGA-GBM] collection [Data set]. The cancer imaging archive. 2016. https://doi.org/10.7937/K9/TCIA.2016.RNYFUYE9
37. Baid U, Ghodasara S, Mohan S,Bilello M, Calabrese E, Colak E, Farahani K, Kalpathy-Cramer J, Kitamura FC. The RSNA-ASNR-MICCAI BraTS 2021 benchmark on brain tumor segmentation and radiogenomic classification. arXiv:2107.02314v2 [cs.CV]. 2021. https://doi.org/10.48550/arXiv.2107.02314
38. Menze BH, Jakab A, Bauer S, Kalpathy-Cramer J, Farahani K, Kirby J, Burren Y, Porz N, Slotboom J. The multimodal brain tumor image segmentation benchmark (BRATS). IEEE Trans Med Imaging. 2014;34:1993–2024
39. Bakas S, Akbari H, Sotiras A, Bilello M, Rozycki M, Kirby JS, Freymann JB, Farahani K, Davatzikos C. Advancing the cancer genome atlas glioma MRI collections with expert segmentation labels and radiomic features. Sci Data. 2017;4:170117
40. Weller M, Stupp R, Reifenberger G, Brandes AA, van den Bent MJ, Wick W, Hegi ME. MGMT promoter methylation in malignant gliomas: ready for personalized medicine? Nat Rev Neurol. 2010;6:39–51
41. Yu W, Zhang L, Wei1 Q, Shao A. O6-methylguanine-DNA methyltransferase (MGMT): challenges and new opportunities in glioma chemotherapy. Front Oncol. 2020;9:1547
42. Horn D, Gottlieb A. Algorithm for data clustering in pattern recognition problems based on quantum mechanics. Phys Rev Lett. 2002;88:018702
43. Weinstein M, Horn D. Dynamic quantum clustering: a method for visual exploration of structures in data. Phys Rev E 2009;80:066117

44. Sánchez J, Martín-Landrove M. A dynamic quantum clustering approach to brain tumor segmentation. arXiv:2107.07698v2 [physics.med-ph]; 2021
45. Sánchez J, Martín-Landrove M. Morphological and fractal properties of brain tumors. Front Physiol 2022;13:878391
46. Lafata K, Zhou Z, Liu J-G, Yin F-F. Data clustering based on Langevin annealing with a self-consistent potential. arXiv:1806.10597v1 [physics.comp-ph]; 2018
47. Kantelhardt JW, Zschiegner SA, Koscielny-Bunde E, Havlin S, Bunde A, Stanley HE. Multifractal detrended fluctuation analysis of nonstationary time series. Phys A Stat Mech Its Appl 2002;316:87–114
48. Lopes R, Betrouni N. Fractal and multifractal analysis: A review. Medical Image Analysis 2009;13:634–649
49. Gu G-F, Zhou W-X. Detrended fluctuation analysis for fractals and multifractals in higher dimensions. Phys Rev E 2006;74:061104